

LYMAN α DOMINANCE OF THE CLASSICAL T TAURI FUV RADIATION FIELD

REBECCA SCHINDHELM¹, KEVIN FRANCE², GREGORY J. HERCZEG³, EDWIN BERGIN⁴, HAO YANG⁵, ALEXANDER BROWN²,
JOANNA M. BROWN⁶, JEFFREY L. LINSKY⁷, JEFF VALENTI⁸

Draft version September 15, 2021

ABSTRACT

Far-ultraviolet (FUV) radiation plays an important role in determining chemical abundances in protoplanetary disks. H I Lyman α is suspected to be the dominant component of the FUV emission from Classical T Tauri Stars (CTTSs), but is difficult to measure directly due to circumstellar and interstellar H I absorption. To better characterize the intrinsic Lyman α radiation, we present FUV spectra of 14 CTTSs taken with the *Hubble Space Telescope* COS and STIS instruments. H₂ fluorescence, commonly seen in the spectra of CTTSs, is excited by Lyman α photons, providing an indirect measure of the Lyman α flux incident upon the warm disk surface. We use observed H₂ progression fluxes to reconstruct the CTTS Lyman α profiles. The Lyman α flux correlates with total measured FUV flux, in agreement with an accretion-related source of FUV emission. With a geometry-independent analysis, we confirm that in accreting T Tauri systems Lyman α radiation dominates the FUV flux ($\sim 1150 \text{ \AA} - 1700 \text{ \AA}$). In the systems surveyed this one line comprises 70 - 90 % of the total FUV flux.

Subject headings: stars: pre-main sequence

1. INTRODUCTION

One of the most influential factors in determining the local composition and physical state of the gas in protoplanetary disks is the ultraviolet (UV) radiation field. Strong UV radiation is produced from hot gas in the magnetically active atmospheres of the central star, and at the magnetospheric shock where disk material collides with the stellar atmosphere (Günther & Schmitt 2008; Sacco et al. 2008). UV photons have a profound influence on the gas heating (Jonkheid et al. 2004; Nomura et al. 2007; Voitke et al. 2009) and disk gas chemistry (Aikawa & Herbst 1999; Bethell & Bergin 2009; Fogel et al. 2011). Surveys of the UV radiation field have been able to characterize the general spectral structure of the radiation (Valenti et al. 2000; Yang et al. 2012). H I Lyman α (Ly α) is a significant contributor to the UV radiation, comprising as much as 80% of the far-UV (FUV) emission produced in the stellar atmosphere and accretion shock (Bergin et al. 2003; Herczeg et al. 2004). While the Ly α radiation is intense close to the star, atomic hydrogen in the disk atmosphere at larger radii isotropically scatters Ly α photons which provides greater penetration into the molecular disk. This is quite different from UV photons at other wavelengths that are scattered solely by dust grains, leading to a Ly α dominated radiation

field - if Ly α radiation is present (Herczeg 2005; Bethell & Bergin 2011). This is important because Ly α dissociates many molecules such as H₂O and CH₄, and can lead to an overabundance of certain species, especially CN (Bergin et al. 2003; van Zadelhoff et al. 2003; van Dishoeck et al. 2006).

While many strong UV transitions such as C IV and He II have been studied (Ingleby et al. 2011; Yang et al. 2012), an intrinsic Ly α profile has only been well characterized in a single Classical T Tauri Star (CTTS) - TW Hya (Herczeg et al. 2004). Due to circumstellar and interstellar H I absorption, it is impossible to directly measure the intrinsic Ly α emission of most CTTSs. On the other hand, H₂ emission resulting from Ly α photoexcitation is prevalent throughout the FUV bandpass, providing an indirect probe of the Ly α . Several Lyman and Werner band transitions reside at wavelengths coincident with the Ly α profile, and have a relatively simple radiative transfer. These lines have been identified in previous observations of CTTSs (Brown et al. 1981; Valenti et al. 2000; Ardila et al. 2002; Herczeg et al. 2002, 2006; France et al. 2011a). H₂ emission therefore provides an opportunity to study the circumstellar region where the Ly α radiation interacts with the disk molecular gas, as well as characterize the strength of this key component of the FUV radiation field in T Tauri systems.

The impact of strong Ly α radiation on disks has only recently been explored in detailed UV radiation transfer models (Bethell & Bergin 2011) and chemical models (Fogel et al. 2011). Given the influence of these photons on gas throughout the disk, quantifying the Ly α emission in CTTSs is crucial to produce accurate disk thermal/chemistry models. In this letter, we reconstruct the Ly α profile from observed H₂ emission lines in the FUV spectra of CTTSs.

2. OBSERVATIONS

Our sample includes 14 CTTSs, chosen for their strong H₂ and FUV continuum emission. The targets, as well as their distances and extinctions, are listed in Table 1. We

¹ Southwest Research Institute, 1050 Walnut St., Suite 300, Boulder, CO 80303, USA; RSCHINDH@ball.com

² Center for Astrophysics and Space Astronomy, University of Colorado, 389 UCB, Boulder, CO 80309, USA

³ Kavli Institute for Astronomy and Astrophysics, Peking University, Beijing 100871, China

⁴ Department of Astronomy, University of Michigan, 830 Denison Building, 500 Church Street, Ann Arbor, MI 48109, USA

⁵ Institute of Astrophysics, Central China Normal University, Wuhan, Hubei, 430079, China

⁶ Harvard-Smithsonian Center for Astrophysics, 60 Garden Street, MS-78, Cambridge, MA 02138, USA

⁷ JILA, University of Colorado and NIST, 440 UCB, Boulder, CO 80309, USA

⁸ Space Telescope Science Institute, 3700 San Martin Drive, Baltimore MD, 21218, USA

adopt target and line-of-sight parameters from France et al. (2012). Most observations utilized the G130M and G160M medium resolution ($\Delta v \approx 17 \text{ km s}^{-1}$) modes of COS (Green et al. 2012). We also use archival STIS E140M observations of TW Hya from the StarCAT spectral catalog (Ayres 2010) to compare our results with previous analysis (Herczeg et al. 2004).

This sample includes targets from the Taurus-Auriga, η Chamaeleontis, and TW Hya star-forming regions, in addition to isolated systems. They are a subset of a full CTTS H_2 survey presented in more detail in France et al. (2012). All the CTTSs in our sample display $\text{Ly}\alpha$ -excited H_2 emission lines throughout the COS bandpass with an average line width of $46 \pm 14 \text{ km s}^{-1}$. Circumstellar and interstellar H I absorbs the $\text{Ly}\alpha$ profiles to varying degrees in each target. Figure 1 shows the observed H_2 emission and $\text{Ly}\alpha$ profiles of several targets. An H I component absorbs the $\text{Ly}\alpha$ line core in V4046 Sgr, while an outflow absorber attenuates most of the short wavelength side of the $\text{Ly}\alpha$ profile of RU Lupi. Very little $\text{Ly}\alpha$ emission is observed in the DE Tau spectra. However, each target shows abundant $\text{Ly}\alpha$ excited H_2 emission lines (France et al. 2012), demonstrating that the observed $\text{Ly}\alpha$ profile can vastly underrepresent the local $\text{Ly}\alpha$ radiation field at the disk surface.

3. ANALYSIS

Wood et al. (2002) and Herczeg et al. (2004) developed a method of $\text{Ly}\alpha$ reconstruction using photo-excited H_2 emission lines in the UV spectra of Mira B and TW Hya. The line fluxes were used in fluorescence models to determine the intrinsic $\text{Ly}\alpha$ profiles and H_2 properties of each object. To make an analysis of a larger sample tractable, we employ a similar technique with only the brightest H_2 progressions. A progression refers to the cascade of electronic transitions originating from an individual rotational-vibrational level of the excited electronic state. Similar to the previous studies, we first measure the H_2 lines, and then model the $\text{Ly}\alpha$ profiles.

3.1. H_2 Emission Spectra and the Absorbed $\text{Ly}\alpha$ Flux

We employed a multi-Gaussian IDL line-fitting code, optimized for COS emission line spectra, to measure the total flux from $\text{Ly}\alpha$ -pumped H_2 . This code assumes a Gaussian line-shape convolved with a wavelength dependent line spread function (LSF), then uses the MPFIT routine to minimize χ^2 between the fit and data (Markwardt 2009). An unconvolved Gaussian was used for TW Hya observed with STIS. To reconstruct the local $\text{Ly}\alpha$ profile incident upon the molecular disk surface, we measured the total flux from 12 fluorescent progressions excited by $\text{Ly}\alpha$. We chose to restrict the emission line analysis to the 1395 – 1640 Å range to mitigate the effects of H_2 self-absorption, which are strongest at $\lambda \lesssim 1400 \text{ Å}$ (Herczeg et al. 2004). The brightest, unblended lines from 12 progressions in the 1395 – 1640 Å bandpass (up to 38 lines) were fitted. We refer the reader to France et al. (2012) for additional information on the H_2 emission characteristics of our sample, including progression IDs for all lines measured.

The total flux from progression m is given by

$$F_m = \frac{1}{N} \sum \left(\frac{F_{mn}}{B_{mn}} \right) \quad (1)$$

where F_{mn} is the reddening corrected, integrated H_2 emission line flux (in units of $\text{ergs cm}^{-2} \text{ s}^{-1}$) from rovibrational state m ($= [v', J']$) in the $B^1\Sigma_u^+$ electronic state to n ($= [v'', J'']$) in the ground electronic state, $X^1\Sigma_g^+$. B_{mn} is the branching ratio for each transition in a progression, defined as the ratio of the Einstein A -value for a given transition $m \rightarrow n$ ($A_{v',J' \rightarrow v'',J''}$) to the total transition rate out of state m , including transitions to bound states and the vibrational continuum (Stecher & Williams 1967; Wood & Karovska 2004; France et al. 2011b). N is the number of emission lines measured from a given progression.

We take the error to be the standard deviation of the individual measurements of $F_m(\text{H}_2)$, as this is the relative uncertainty in H_2 fluxes in most cases. These standard deviations are typically less than 10% for bright progressions, and as high as 20 - 30% in weaker progressions. The primary uncertainty in H_2 luminosities relates to the extinction correction (see A_V in Table 1), although to zeroth order this would affect all progressions similarly as they have been chosen from a narrow range of wavelengths. Upper limits on the H_2 emission line fluxes of undetectable progressions were determined from the standard deviation in a $\pm 50 \text{ km s}^{-1}$ region surrounding the laboratory wavelength of the transition.

The flux incident on the H_2 ($I_{inc}(\lambda_m)$, in units of $\text{ergs cm}^{-2} \text{ s}^{-1} \text{ Å}^{-1}$) at each H_2 absorbing transition wavelength λ_m was then assumed to be the total progression flux divided by the equivalent width (W_λ) of the absorbing H_2 transition:

$$I_{inc}(\lambda_m) = F_m/W_\lambda \quad (2)$$

$$W_\lambda = \int_\lambda (1 - e^{-\tau_\lambda [T_{H_2}, N_{H_2}]}) d\lambda \quad (3)$$

where each $[v, J]$ state of the ground electronic level is populated by a single rotational temperature (T_{H_2}) and column density (N_{H_2}). Non-thermal populations can result from dust heating and photo excitation by the strong X-ray and UV radiation fields (Nomura et al. 2007; Gorti & Hollenbach 2009). However, a degeneracy exists between T_{H_2} and N_{H_2} in our model, discussed further in Section 3.2. As a first order approximation to simplify this degeneracy we assume a thermal population. To determine W_λ , we used a grid of T_{H_2} in 100 K increments from 1000 K to 5000 K, and N_{H_2} in 0.1 dex increments from 10^{16} to 10^{22} cm^{-2} . Models with $T_{H_2} < 1000 \text{ K}$ produce a negligible population in the $v=2$ level of the ground electronic state and are therefore not considered. For each of the 12 transitions, we calculated a set of I_{inc} for each pair of T_{H_2} and N_{H_2} . Each pair of T_{H_2} and N_{H_2} therefore creates 12 unique values of I_{inc} .

3.2. $\text{Ly}\alpha$ Profile Reconstruction

Our reconstruction technique finds the set of outflow-absorbed $\text{Ly}\alpha$ profiles (I_{ab} , in units of $\text{ergs cm}^{-2} \text{ s}^{-1} \text{ Å}^{-1}$) that best fit the variety of I_{inc} values. The model assumes $\text{Ly}\alpha$ emission is created near the stellar surface. Some amount of H I lies in between the $\text{Ly}\alpha$ source and the H_2 , absorbing some of the $\text{Ly}\alpha$ photons before they reach the H_2 . For each target, we create a grid of I_{ab}

Table 1
Target Properties and Fluxes

Target	A_V	d (pc)	$\langle F_{Ly\alpha} \rangle^a$	$\langle F_{ab} \rangle^b$	FWHM (km s $^{-1}$) ^c	N_{out} (10 19 cm $^{-2}$) ^c	v_{out} (km s $^{-1}$) ^c	F_{FUV}^d
AA Tau	0.5	140	35.2 \pm 6.3	16.5 \pm 2.4	642 \pm 33	1.11 \pm 0.31	-143 \pm 16	3.5
BP Tau	0.5	140	31.5 \pm 5.5	20.7 \pm 3.0	613 \pm 54	0.44 \pm 0.30	-131 \pm 29	14.1
DE Tau	0.6	140	15.4 \pm 4.5	7.91 \pm 2.8	623 \pm 75	0.92 \pm 0.53	-156 \pm 28	3.6
DM Tau	0.0	140	4.6 \pm 0.5	3.19 \pm 0.4	912 \pm 35	0.39 \pm 0.03	-89 \pm 4	1.1
GM Aur	0.1	140	12.2 \pm 3.0	6.19 \pm 1.5	815 \pm 31	1.16 \pm 0.32	-129 \pm 17	2.9
HN Tau	0.5	140	12.9 \pm 2.6	7.08 \pm 1.4	776 \pm 40	1.15 \pm 0.49	-153 \pm 26	2.8
LkCa 15	0.6	140	17.2 \pm 2.8	9.54 \pm 2.0	665 \pm 39	0.80 \pm 0.40	-139 \pm 25	3.0
RECX 11	0.0	97	5.2 \pm 0.4	3.07 \pm 0.6	573 \pm 63	0.78 \pm 0.48	-126 \pm 35	0.8
RECX 15	0.0	97	11.6 \pm 1.6	5.73 \pm 1.0	848 \pm 54	0.96 \pm 0.38	-125 \pm 27	1.0
RU Lupi	0.1	150	23.4 \pm 5.5	10.3 \pm 1.7	707 \pm 59	3.14 \pm 1.56	-219 \pm 52	7.5
SU Aur	0.9	140	35.4 \pm 8.2	14.8 \pm 1.9	644 \pm 59	2.34 \pm 1.37	-177 \pm 47	6.9
TW Hya	0.0	56	52.5 \pm 9.1	38.3 \pm 6.6	865 \pm 35	0.29 \pm 0.12	-77 \pm 16	41.4
UX Tau	0.2	140	6.2 \pm 0.5	4.32 \pm 0.4	606 \pm 42	0.18 \pm 0.04	-64 \pm 7	1.1
V4046 Sgr	0.0	83	46.0 \pm 5.1	24.9 \pm 2.2	627 \pm 38	0.65 \pm 0.26	-108 \pm 17	7.0

Fluxes in 10 $^{-12}$ ergs cm $^{-2}$ s $^{-1}$

^a Intrinsic, unabsorbed model flux

^b H $_2$ -incident, circumstellar H I-absorbed model flux

^c Average parameters of intrinsic model Ly α profiles

^d Integrated 1160 - 1695 Å flux, excluding Ly α (1207 - 1222 Å) and O I (1300 - 1310 Å).

profiles, each with its own single Gaussian emission component and single outflow H I absorber:

$$I_{ab} = (C_{Ly\alpha} + I_{Ly\alpha})e^{-\tau_{out}} \quad (4)$$

$C_{Ly\alpha}$ is the average continuum flux per Angstrom near Ly α . $I_{Ly\alpha}$ is the accretion/magnetospheric-generated Gaussian emission profile, centered at the stellar radial velocity and parameterized by amplitude I_0 and FWHM (in units of ergs cm $^{-2}$ s $^{-1}$ Å $^{-1}$ and km s $^{-1}$, respectively). The optical depth τ_{out} is determined with a Voigt profile for the H I Ly α transition, characterized by an outflow velocity v_{out} and column density N_{out} (in units of km s $^{-1}$ and cm $^{-2}$, respectively). This outflow absorption component is essential to adequately fitting the I_{inc} values.

For each I_{ab} model profile, a χ^2 is calculated with each set of [T_{H_2}, N_{H_2}]-dependent I_{inc} . We then exclude any sets of T_{H_2} and N_{H_2} which yield a χ^2 greater than 95.4% (2σ) from the peak of the χ^2 probability distribution. The H $_2$ progressions for which only upper limits are calculated provide additional constraints on the Ly α profile; we reject any Ly α profile with a flux greater than an upper limit value at that wavelength. Given the various combinations of I_0 , FWHM, v_{out} , N_{out} , T_{H_2} , and N_{H_2} , a variety of Ly α profiles adequately fit the I_{inc} values. This is demonstrated in Figure 1, where several combinations of $I_{Ly\alpha}$, I_{ab} , and I_{inc} are shown. We quantify the overall distribution of $I_{Ly\alpha}$ profiles for each target by integrating each $I_{Ly\alpha}$ profile from 1210 Å to 1222 Å, resulting in fluxes $F_{Ly\alpha}$ (in units of ergs cm $^{-2}$ s $^{-1}$) which form an approximately Gaussian distribution.

The average $F_{Ly\alpha}$ ($\langle F_{Ly\alpha} \rangle$) of each target is listed in Table 1, along with the 1σ width of the distribution. $\langle F_{Ly\alpha} \rangle$ represents the total Ly α flux at the star, and is generally constrained to within 10 - 20 %. We also include the average emission FWHM and H I absorber properties (N_{out} and v_{out}). Integrating I_{ab} , the H $_2$ -incident Ly α flux, yields $\langle F_{ab} \rangle$. Assuming a thermally populated ground state distribution, typical T_{H_2}

values are $\sim 2500 \pm 1000$ K and $\log(N_{H_2}(\text{cm}^{-2})) \sim 19 \pm 1$, similar to those found in TW Hya (Herczeg et al. 2004). Strong UV and X-ray irradiation from the central star would act to preferentially populate excited rovibrational levels in excess of the thermal distribution (see e.g., Nomura et al. (2007)). In our simple model, non-thermal excitation would be approximated by higher rotational temperatures, and this increase in rovibrational population will be offset by lower total H $_2$ column densities. The varying effects of non-thermal excitation most likely contribute to the spread of the observed N_{H_2} and T_{H_2} values. Lower N_{H_2} can require increased Ly α flux, although we expect that this increase will be of the same order of the uncertainty on the derived Ly α emission flux ($\sim 10 - 20$ %). Untangling the effects of non-thermal populations requires more complex modeling, including the effects of H $_2$ formation on dust grains, and disk modeling efforts that predict the UV fluorescent spectrum of H $_2$ (and CO) would be very valuable. Regardless, the overall model Ly α properties follow approximately gaussian distributions. Figure 2 compares $\langle F_{Ly\alpha} \rangle$ and the observed Ly α fluxes (F_{obs} , summed over the entire profile) with the total H $_2$ fluxes. F_{obs} has a Spearman ρ rank correlation coefficient of 0.57 while $\langle F_{Ly\alpha} \rangle$, by design, has a ρ of 0.96.

Ideally we would compare our model Ly α profiles with the observed Ly α profiles. However, this involves additional parameters and a more complex analysis than presented here. Primarily, the radiative transfer of Ly α photons between the source, the H $_2$, and Earth must account for the geometric filling fraction η . This fraction represents the solid angle of H $_2$ illuminated by the Ly α emission, such that $\eta=1$ implies the H $_2$ completely surrounds the star. An η other than 1 would enter Equation 2 by multiplying $I_{inc}(\lambda_m)$ by η . Herczeg et al. (2004) found $\eta=0.25$ for TW Hya, implying gas in a disk surface layer. However, Wood et al. (2002) measured $\eta > 2$ in Mira B. A filling factor greater than 1 would possibly correspond to preferential scattering of H $_2$ photons

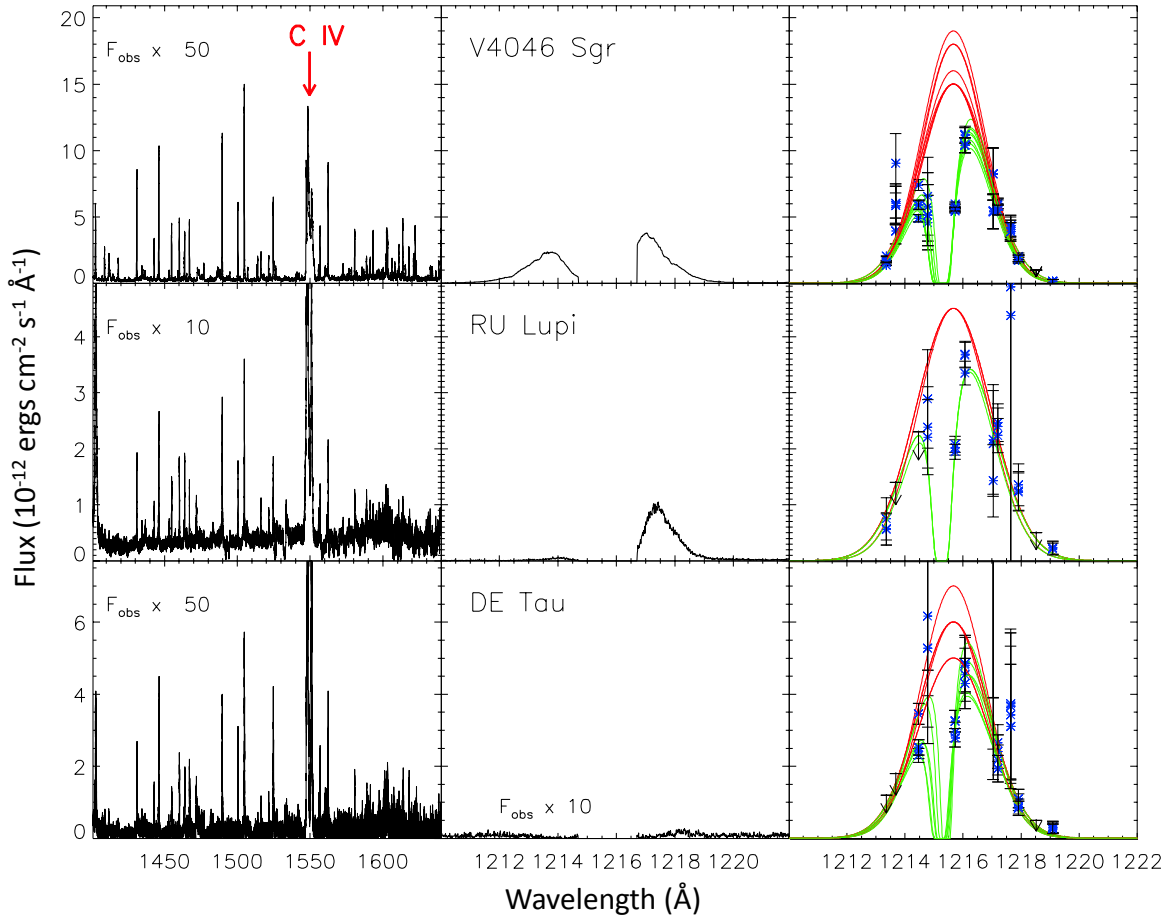


Figure 1. Observed and model spectra for V4046 Sgr (top row), RU Lupi (middle row), and DE Tau (bottom row). H_2 emission lines are present throughout the FUV (left column), regardless of whether or not the photo-exciting $Ly\alpha$ is observed (middle). In RU Lupi, a circumstellar wind extinguishes most of the short wavelength side of the $Ly\alpha$ profile, while in DE Tau $Ly\alpha$ is completely absorbed. We use the photo-excited H_2 lines to reconstruct model $Ly\alpha$ profiles (right). Each pair of intrinsic ($I_{Ly\alpha}$, red) and outflow-absorbed (I_{ab} , green) profiles are a best fit to a different set of $[N_{H_2}, T_{H_2}]$ -based incident fluxes (I_{inc} , blue asterisks).

into, or more likely $Ly\alpha$ photons out of, our line of sight (Wood et al. 2002). Future analysis will incorporate η into a more detailed radiative transfer model of our sample targets.

3.3. Total $Ly\alpha$ Flux in CTTSs

We determine the fraction of the total FUV output from CTTSs that is in the $Ly\alpha$ emission line, adopting a definition of the $Ly\alpha$ fraction, $f_{Ly\alpha}$, given by

$$f_{Ly\alpha} = \frac{F_{Ly\alpha}}{(F_{FUV} + F_{Ly\alpha})} \quad (5)$$

where $F_{Ly\alpha}$ is our average model $Ly\alpha$ flux from the star (in units of $\text{ergs cm}^{-2} \text{s}^{-1}$; §3.2) and F_{FUV} is the total unreddened FUV flux, measured over the 1160 – 1695 Å bandpass (in units of $\text{ergs cm}^{-2} \text{s}^{-1}$). The wings of the stellar $Ly\alpha$ can extend to $> \pm 1000 \text{ km s}^{-1}$ from line center in some targets (see e.g, Figure 2 (top) from Yang et al. 2011), therefore we excluded the 1207 – 1225 Å region from the computation of F_{FUV} . We also excluded the 1300 – 1310 Å region to remove contamination by the geocoronal O I multiplet. A 5% error is assumed on

F_{FUV} corresponding to the uncertainty in flux calibration. The restriction of the total FUV band to 1160 – 1695 Å is mainly driven by the lack of supporting *FUSE* observations at short wavelengths (912 – 1160 Å) for all targets and the end of the STIS E140M bandpass at 1700 Å.

Molecular line emission from H_2 (Herczeg et al. 2006; this work) and CO (France et al. 2011a; Schindhelm et al. 2012) contributes to F_{FUV} . The FUV molecular emission is thought to originate from an inner warm disk surface ($a \leq 3 \text{ AU}$) (Herczeg et al. 2004; France et al. 2012) or outflow (Saucedo et al. 2003; Walter et al. 2003). The total FUV flux also includes a molecular continuum whose excitation mechanism and spatial distribution are not well constrained (Bergin et al. 2004; France et al. 2011b). $\langle F_{Ly\alpha} \rangle$ shows a much better correlation with F_{FUV} than F_{obs} (Figure 2). This is consistent with the idea that both the $Ly\alpha$ and FUV continuum emission are produced by related processes.

We also calculate an observed $Ly\alpha$ fraction (f_{obs}) using F_{obs} instead of $F_{Ly\alpha}$ in Equation 5. We compare f_{obs} and $f_{Ly\alpha}$ with the total H_2 flux in Figure 3. For our general assumption of $\eta=1$, we find an average $\langle f_{Ly\alpha} \rangle$

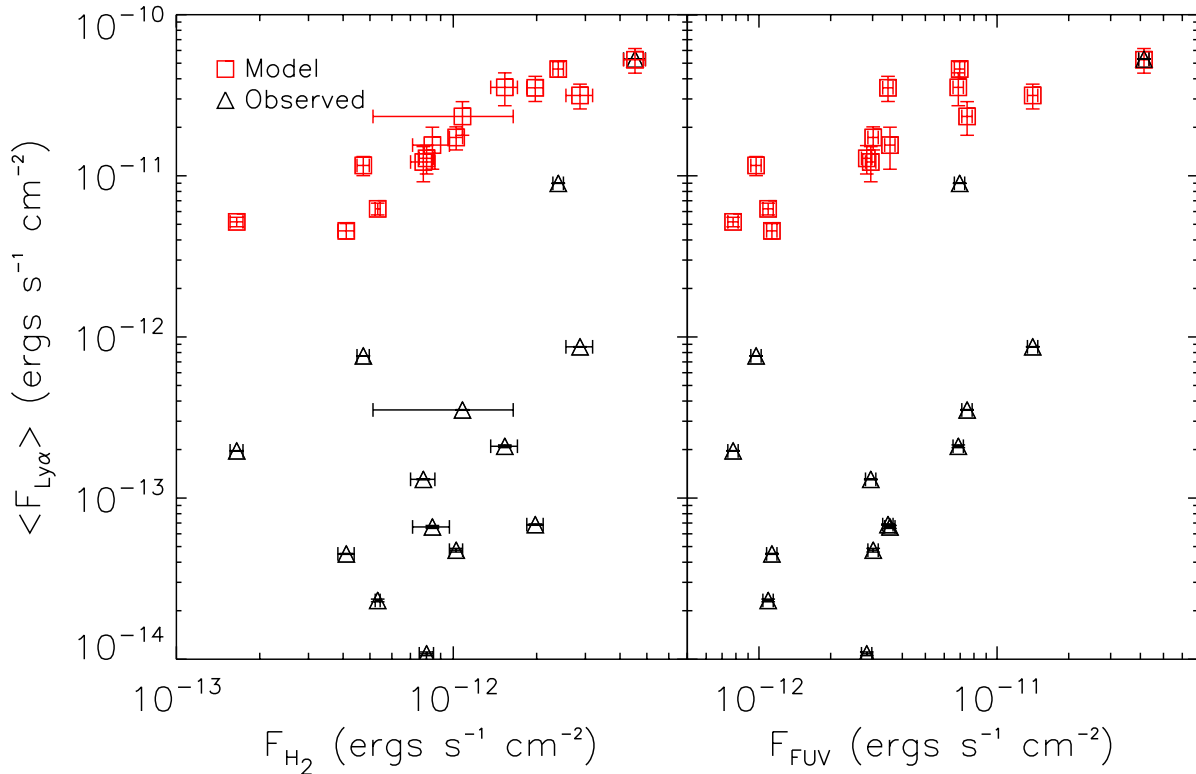


Figure 2. Integrated model (squares) and observed (triangles) Ly α flux vs. total H $_2$ flux (left) and total FUV flux (right) for each target. The total H $_2$ flux is calculated by summing all the progression fluxes measured in our analysis. F_{FUV} is the total unreddened FUV flux measured over the 1160 – 1695 Å bandpass.

of $81 \pm 9\%$, compared with $15^{+21}_{-15}\%$ for $\langle f_{obs} \rangle$. For $\eta = 0.1, 0.25, 0.5,$ and 2.0 , $\langle f_{Ly\alpha} \rangle$ is 97%, 94%, 90%, and 69%, respectively. A slight trend for decreasing $\langle f_{Ly\alpha} \rangle$ with increasing F_{FUV} is apparent, although this may be inappropriately weighted by BP Tau and TW Hya. Regardless, our calculated $\langle f_{Ly\alpha} \rangle$ values demonstrate the validity of previous assertions that Ly α emission dominates the FUV radiation field from CTTs (e.g. Bergin et al. (2003)).

4. DISCUSSION AND CONCLUSIONS

We have demonstrated that Ly α dominates the FUV emission of CTTs. Ly α -fluoresced H $_2$ emission lines appear throughout the spectra of each CTTs in our survey. Circumstellar and interstellar H I partially attenuates the line centers of the Ly α profiles in most targets and completely absorbs them in several targets. The *observed* Ly α fluxes do not correlate with either the total H $_2$ emission or the summed FUV continuum flux. The strongest fluorescent H $_2$ progressions are used to reconstruct the Ly α profile incident on the molecular disk, yielding $F_{Ly\alpha}$ values accurate to within $\sim 20\%$ in most targets. This uncertainty is caused by the distribution of possible H I and H $_2$ properties. Our model assumptions (such as a single Gaussian emission component or simple outflow absorber) may hide larger systematic errors, however future work will study these effects in a more detailed model. We find that the intrinsic Ly α comprises $81 \pm 9\%$ of the total FUV emission from CTTs, compared with a fraction of only $15^{+21}_{-15}\%$ for the observed Ly α profiles. This demonstrates the need for Ly α reconstruction to achieve accurate disk models of CTTs.

It is clear from our results that the detection of the strong Ly α line in TW Hya was not limited to a single object. Rather, strong Ly α emission dominates the FUV flux from all accreting (classical) T Tauri stars. Our measurements of the relative Ly α /FUV continuum flux only compare Ly α to the FUV flux from 1160 - 1695 Å. Thus if there is significant UV flux shortward of 1160 Å then the strength of Ly α relative to the FUV radiation could go down. However, in TW Hya the flux below this limit is only 5% of the FUV flux below 1700 Å. Similarly, France et al. (2011b) have shown that the FUV continuum decreases to shorter wavelengths across the FUV bandpass. In addition, the absorption properties of grains strongly limit the propagation of UV photons near the Lyman limit.

The derived Ly α fractions confirm the dominance of Ly α in the FUV spectrum of the accreting young stars with disks. This is important because Ly α photons from the star will see the atomic hydrogen layer, with shallow angle of incidence, above the molecular surface. Isotropic scattering will lead a significant fraction of the Ly α flux to rain down on the disk with greater penetrating power than typical UV continuum photons (Bethell & Bergin 2011). In addition, the Ly α emission reprocessed by H $_2$ (which is scattered throughout the FUV spectrum) will also emit directly on the disk surface (France et al. 2012). These two effects increase the penetration of UV photons beyond the simple case where one assumes the UV photons observe the disk surface with shallow angle of incidence and with the propagation solely influenced by grains. In general this should lead to greater heating and

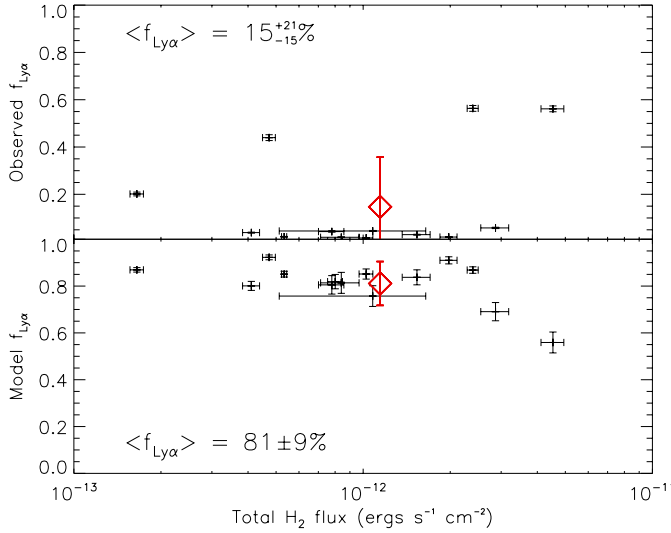


Figure 3. Observed (top) and model (bottom) Ly α fraction (assuming $\eta=1$) vs. total H $_2$ flux. The diamond in each plot designates the average $f_{Ly\alpha}$ value for the observed and model profiles. The significant increase in Ly α fraction from the observed to the model profiles demonstrates the importance of Ly α reconstruction.

additional chemical effects deeper in the disk system.

RS and KF thank Brian Wood for input on Ly α profile reconstruction. This work was supported by NASA grants NNX08AC146 and NAS5-98043 to the University of Colorado at Boulder (*HST* programs 11533 and 12036) and made use of data from *HST* GO programs 8041 and 11616.

REFERENCES

- Aikawa, Y. & Herbst, E. 1999, *A&A*, 351, 233
Ardila, D. R., Basri, G., Walter, F. M., Valenti, J. A., & Johns-Krull, C. M. 2002, *ApJ*, 566, 1100
Ayres, T. R. 2010, *ApJS*, 187, 149
Bergin, E., Calvet, N., D'Alessio, P., & Herczeg, G. J. 2003, *ApJ*, 591, L159
Bergin, E., Calvet, N., Sitko, M. L., Abgrall, H., D'Alessio, P., Herczeg, G. J., Roueff, E., Qi, C., Lynch, D. K., Russell, R. W., Brafford, S. M., & Perry, R. B. 2004, *ApJ*, 614, L133
Bethell, T. & Bergin, E. 2009, *Science*, 326, 1675
Bethell, T. J. & Bergin, E. A. 2011, *ApJ*, 739, 78
Brown, A., Jordan, C., Millar, T. J., Gondhalekar, P., & Wilson, R. 1981, *Nature*, 290, 34
Fogel, J. K. J., Bethell, T. J., Bergin, E. A., Calvet, N., & Semenov, D. 2011, *ApJ*, 726, 29
France, K., Schindhelm, R., Burgh, E. B., Herczeg, G. J., Harper, G. M., Brown, A., Green, J. C., Linsky, J. L., Yang, H., Abgrall, H., Ardila, D. R., Bergin, E., Bethell, T., Brown, J. M., Calvet, N., Espaillat, C., Gregory, S. G., Hillenbrand, L. A., Hussain, G., Ingleby, L., Johns-Krull, C. M., Roueff, E., Valenti, J. A., & Walter, F. M. 2011a, *ApJ*, 734, 31
France, K., Schindhelm, R., Herczeg, G. J., Brown, A., Abgrall, H., Alexander, R. D., Bergin, E. A., Brown, J. M., Linsky, J. L., Roueff, E., & Yang, H. 2012, *ArXiv e-prints*
France, K., Yang, H., & Linsky, J. L. 2011b, *ApJ*, 729, 7
Gorti, U. & Hollenbach, D. 2009, *ApJ*, 690, 1539
Green, J. C., Froning, C. S., Osterman, S., Ebbets, D., Heap, S. H., Leitherer, C., Linsky, J. L., Savage, B. D., Sembach, K., Shull, J. M., Siegmund, O. H. W., Snow, T. P., Spencer, J., Stern, S. A., Stocke, J., Welsh, B., Béland, S., Burgh, E. B., Danforth, C., France, K., Keeney, B., McPhate, J., Penton, S. V., Andrews, J., Brownsberger, K., Morse, J., & Wilkinson, E. 2012, *ApJ*, 744, 60
Günther, H. M. & Schmitt, J. H. M. M. 2008, *A&A*, 481, 735
Herczeg, G. J. 2005, PhD thesis, University of Colorado at Boulder, Colorado, USA
Herczeg, G. J., Linsky, J. L., Valenti, J. A., Johns-Krull, C. M., & Wood, B. E. 2002, *ApJ*, 572, 310
Herczeg, G. J., Linsky, J. L., Walter, F. M., Gahm, G. F., & Johns-Krull, C. M. 2006, *ApJS*, 165, 256
Herczeg, G. J., Wood, B. E., Linsky, J. L., Valenti, J. A., & Johns-Krull, C. M. 2004, *ApJ*, 607, 369
Ingleby, L., Calvet, N., Hernández, J., Briceño, C., Espaillat, C., Miller, J., Bergin, E., & Hartmann, L. 2011, *AJ*, 141, 127
Jonkheid, B., Faas, F. G. A., van Zadelhoff, G.-J., & van Dishoeck, E. F. 2004, *A&A*, 428, 511
Markwardt, C. B. 2009, in *Astronomical Society of the Pacific Conference Series*, Vol. 411, *Astronomical Data Analysis Software and Systems XVIII*, ed. D. A. Bohlender, D. Durand, & P. Dowler, 251
Nomura, H., Aikawa, Y., Tsubimoto, M., Nakagawa, Y., & Millar, T. J. 2007, *ApJ*, 661, 334
Sacco, G. G., Argiroffi, C., Orlando, S., Maggio, A., Peres, G., & Reale, F. 2008, *A&A*, 491, L17
Saucedo, J., Calvet, N., Hartmann, L., & Raymond, J. 2003, *ApJ*, 591, 275
Schindhelm, R., France, K., Burgh, E. B., Herczeg, G. J., Green, J. C., Brown, A., Brown, J. M., & Valenti, J. A. 2012, *ApJ*, 746, 97
Stecher, T. P. & Williams, D. A. 1967, *ApJ*, 149, L29+
Valenti, J. A., Johns-Krull, C. M., & Linsky, J. L. 2000, *ApJS*, 129, 399
van Dishoeck, E. F., Jonkheid, B., & van Hemert, M. C. 2006, *Faraday Discussions*, 133, 231
van Zadelhoff, G.-J., Aikawa, Y., Hogerheijde, M. R., & van Dishoeck, E. F. 2003, *A&A*, 397, 789
Walter, F. M., Herczeg, G., Brown, A., Ardila, D. R., Gahm, G. F., Johns-Krull, C. M., Lissauer, J. J., Simon, M., & Valenti, J. A. 2003, *AJ*, 126, 3076
Woitke, P., Kamp, I., & Thi, W.-F. 2009, *A&A*, 501, 383
Wood, B. E. & Karovska, M. 2004, *ApJ*, 601, 502
Wood, B. E., Karovska, M., & Raymond, J. C. 2002, *ApJ*, 575, 1057
Yang, H., Herczeg, G. J., Linsky, J. L., Brown, A., Johns-Krull, C. M., Ingleby, L., Calvet, N., Bergin, E., & Valenti, J. A. 2012, *ApJ*, 744, 121
Yang, H., Linsky, J. L., & France, K. 2011, *ApJ*, 730, L10+